A single domain intrabody targeting the follicle-stimulating hormone receptor (FSHR) impacts FSH-induced G protein-dependent signalling

Pauline Raynaud[1], Vinesh Jugnarain[1], Océane Vaugrente[1], Amandine Vallet[1], Thomas Boulo[1], Camille Gauthier[1], Christophe Gauthier[1], Frédéric Jean-Alphonse[1,2], Eric Reiter[1,2], Pascale Crépieux[1,2]*, Gilles Bruneau[1]*

[1]Physiologie de la Reproduction et des Comportements (PRC), Institut National de Recherche pour l'Agriculture, l'Alimentation et l'Environnement (INRAE), Centre National de la Recherche Scientifique (CNRS), Institut Français du Cheval et de l'Equitation (IFCE), Université de Tours, 37380 Nouzilly, France

[2]Inria, Inria Saclay-Ile-de-France, 91120 Palaiseau, France

*Corresponding authors:

Dr. Gilles Bruneau, UMR Physiologie de la Reproduction et des Comportements, Centre de Recherches INRAE Val de Loire, F-37380 Nouzilly, France. E-Mail: Gilles.Bruneau@inrae.fr

Dr. Pascale Crépieux, UMR Physiologie de la Reproduction et des Comportements, Centre de Recherches INRAE Val de Loire, F-37380 Nouzilly, France. E-Mail: Pascale.Crepieux@inrae.fr

Abstract

Intracellular variable fragments from camelid heavy-chain only antibody (intra-VHH) have been successfully used as chaperones to solve the 3D structure of active G protein-coupled receptors (GPCRs) bound to their transducers. However, their effect on signalling has been poorly explored, although they may provide a better understanding on the relationships between receptor conformation and activity. Here, we isolated and characterized iPRC1, the first intra-VHH recognizing a member of the large glycoprotein hormone receptor family, the follicle-stimulating hormone receptor (FSHR). This intra-VHH recognizes the FSHR 3rd intracellular loop and decreases cAMP production in response to FSH, without altering Gαs recruitment. Hence, iPRC1 behaves as an allosteric modulator and provides a new tool to complete structure/activity studies performed so far on this receptor.

Keywords: G protein-coupled receptors, FSH receptor, intracellular VHH, cell signalling

37 **Abbreviations**

38 GPCR: G protein-coupled receptor

39 FSH: Follicle-stimulating hormone

40 FSHR: FSH receptor

41 LHCGR: Luteinizing hormone/choriogonadotropin receptor

42 TSHR: Thyroid-stimulating hormone

43 BSA: Bovine serum albumin

44 BRET: Bioluminescence resonance energy transfer

45 HTRF: Homogeneous time-resolved fluorescence

46 ICL: intracellular loop

47 AVP: Arginine-vasopressin

48 AVPR2: Arginine-vasopressin 2 receptor

49 ISO: Isoproterenol hydrochloride

50 ADRB2: β2 adrenergic receptor

51 Fsk: Forskolin

52 PBS: phosphate-buffered saline

53 APC: Allophycocyanin

54 RLuc8: luciferase from the sea pansy *Renilla reniformis*

55 mini Gs protein: minimal engineered GTPase domain of the Gα subunit

Introduction

G protein-coupled receptors (GPCRs) represent a large family of membrane receptors characterized by an N-terminal extracellular domain, seven transmembrane domains connected by three extracellular and three intracellular loops, and an intracellular C-terminal domain. Ligand binding to a GPCR leads to conformational changes within the transmembrane and intracellular domains, mediating the transduction of an extracellular signal to the interior of the cell. GPCRs are highly dynamic proteins, adopting a plethora of active and inactive conformations (1). This is in accordance with the fact that, upon ligand binding, they are able to interact with a diversity of downstream signalling proteins with variable efficacy. The signal is transduced by heterotrimeric G proteins (Gs, Gi/o, Gq/11, G12/13), G protein-coupled receptor kinases (GRK) and β-arrestins among others. Since GPCRs are involved in the regulation of numerous physiological and pathological processes, regulating their biological activity has been the object of considerable efforts, involving the use of a variety of molecular tools. Ligands recognizing the orthosteric binding site of a GPCR act as agonists or antagonists. The use of allosteric modulators that favour either active (positive allosteric modulator) or inactive (negative allosteric modulator) conformations may fine-tune GPCR signalling. Biased ligands, whether orthosteric or allosteric, exhibit altered efficacy or potency to regulate a specific signalling pathway, when compared to a reference ligand, providing valuable tools to study and control GPCR signalling regulation.

Small molecules have been extensively explored to modulate GPCR signalling and pharmacology, including the FSHR's (2). In the last decade, there has been a growing interest in the development of antibodies targeting GPCRs, especially in the VHH (VH of heavy chain only antibodies) format. These VHHs of low molecular weight (~13 kDa), display the smallest paratope capable of specifically recognizing an epitope. A long and flexible CDR3 that compensates for the absence of light chain enables them to access and recognize cryptic epitopes, such as binding pockets (3). Furthermore, their conformational stability is an advantageous property. VHHs have disulphide bonds not essential for epitope recognition (4), hence they are especially well-suited for intracellular expression despite reducing conditions in the cytosol.

Ligand-bound GPCRs are structurally instable, and the recruitment of transduction proteins (G proteins, β-arrestins) each stabilize a discrete subset of receptor

89 conformations (5). Similarly, intracellular VHHs (intra-VHHs) have the ability to stabilize
90 selective GPCR conformations. Therefore, intra-VHHs targeting GPCRs have been a
91 tremendous help to solve crystal structures of numerous active GPCRs. For example,
92 Nb80 was used as a chaperone to solve crystal structure of the active beta 2
93 adrenergic receptor (ADRB2) (6), Nb9-8 for the structure of active muscarinic
94 acetylcholine receptor M2 (7), or Nb39 for the active structure of mu-opioid receptor
95 (8). All of these intra-VHHs exhibit G protein mimetic properties. Intra-VHHs stabilising
96 partially active conformations of GPCRs have also been identified, such as Nb71
97 targeting ADRB2 (9). Others were able to stabilize inactive conformations, as Nb60,
98 which acts as a negative allosteric modulator at the ADRB2 (10). In addition, some
99 intra-VHHs have been used as biosensors to track GPCR intracellular trafficking. For
100 instance, Nb80 fused to GFP as a biosensor for ADRB2 activation, revealed that active
101 ADRB2 is present at the endosomes (11). Overall, by providing important stabilizing
102 tools, intra-VHHs allowed valuable structural insights on GPCR activation. However,
103 their modulatory impact on GPCR functioning has been poorly explored. So far, few
104 studies reported a functional allosteric effect of intra-VHHs on GPCR signalling, and
105 they are all directed against five GPCRs only (OPRK1, OPRD1, OPEM1, ADRB2 and
106 US28), amongst the 800 members of the family (for review see Raynaud et al., 2022
107 (12)). For example, eighteen intra-VHHs selected on ADRB2 have been functionally
108 characterized and they display variable inhibitory effects on cAMP production and β-
109 arrestin recruitment (13). Four others inhibited the cAMP-responsive element (14).
110 Intra-VHHs used as regulators of GPCR function can provide insight on GPCR
111 signalling and on the receptor regions that are involved.

112 The follicle-stimulating hormone receptor (FSHR) is a class A (rhodopsin-like) GPCR
113 playing a key role in reproduction, by regulating gametogenesis in male and female
114 (15). The FSHR, together with the luteinizing hormone/choriogonadotropin (LHCGR)
115 and thyroid stimulating hormone receptors (TSHR), constitute the subfamily of
116 glycoprotein hormone receptors. Unlike other class A GPCRs, these three receptors
117 are characterized by a large horseshoe-shaped extra-cellular domain, comprising the
118 hormone binding domain (16). The FSH-stimulated FSHR primarily signals through
119 Gs, the Gαs subunit leading to the production of the cAMP second messenger, thus
120 activating protein kinase A (PKA). The Gβγ subunits activate GRKs, which
121 subsequently phosphorylate the receptor on specific motifs, leading notably to the

122 recruitment of β-arrestins (17–19). The latter play a key role in receptor desensitization,
123 internalization and recycling, but also in G protein-independent signalling. FSH-
124 activated FSHR is also engaged with other interaction partners (20), and induces a
125 complex signalling network (21).

126 Through its biological role, the FSHR is a potential target for non-hormonal alternatives
127 to fertility treatments or contraceptives, with the aim of optimizing efficacy while
128 reducing side effects. However, it is not yet clearly understood how a specific signalling
129 pathway correlates with the induced physiological effect. Therefore, to be able to fine-
130 tune FSHR signalling, there is a need for tools allowing to decipher the complexity of
131 the FSHR signalling network. In this study, we isolated a VHH targeting the 3rd
132 intracellular loop of the FSHR, expressed it as an intra-VHH in mammalian cells,
133 showed its binding to the FSHR, and explored its potential modulatory effect on the
134 FSH-induced Gs signalling pathway.

135

136 **Materials and methods**

137 References of the materials are provided in Supplementary Table 1.

138 - *Phage library*

139 The phage library was obtained after intramuscular immunisation of llama with a cDNA
140 encoding the human FSHR (In-Cell-Art, Nantes, France). Total RNAs were extracted
141 from llama circulating leukocytes using LeukoLOCK™ Fractionation & Stabilization Kit
142 (Invitrogen, Waltham, Massachusetts, USA) and reverse-transcribed as cDNA using
143 SuperScript™ III Reverse Transcriptase (Thermo Fisher Scientific, Waltham,
144 Massachusetts, USA). VHHs cDNAs were amplified by nested PCR using Platinum™
145 Taq DNA Polymerase (Thermo Fisher Scientific), as described in Supplementary
146 Figure 1. PCR products were inserted between the SfiI and NotI sites of the pCANTAB
147 6 phagemid vector (kindly provided by Pierre Martineau). The resulting recombinant
148 phagemids were transformed in *E. coli* TG1 bacterial cells (Lucigen, Teddington, UK).
149 Addition of the KM13 helper phage (kindly provided by Pierre Martineau) allowed the
150 production of the phages. The primary library contains 3.10^8 independent phages.

151 - *Phage display*

152 Intra-VHH selection was performed by phage display on each of the three peptides
153 corresponding to the intracellular loops of the human FSHR (ICL1, ICL2 and ICL3).
154 ICL1 (TTSQYKLTVPR), ICL2 (ERWHTITHAMQLDCKVQLRH) and ICL3
155 (HIYLTVRNPNIVSSSSDTRIAKR) peptides were synthetized by Genecust (Boynes,
156 France). Three selection rounds were carried out. For each round of selection, 1 µg of
157 peptide in PBS pH 7.4 was coated into the selection well of Nunc MAXISORP strips
158 (Dutscher, Bernolsheim, France). The first round started with a sample of 10^{11} to 10^{12}
159 phages from the amplified phage library. For rounds 1 and 3, depletion and blocking
160 of nonspecific sites were performed in PBS 2 % bovine serum albumin (BSA) and for
161 round 2, in PBS 2% skimmed milk. Phages were depleted on two wells for 1h, and
162 incubated on the well coated with the peptides for 2 h. Phages were washed 40 times
163 with PBS 0.1 % Tween 20, with one last wash in 50 mM Tris pH 8.0, 1 mM $CaCl_2$. For
164 rounds 1 and 2, phage elution was performed in the latter buffer containing 125 µg/mL
165 bovine trypsin (Sigma-Aldrich, St. Louis, MO, USA), for 15 min at room temperature.
166 For round 3, phages were eluted using 1.5 mM peptide in PBS pH 7.4. TG1 bacterial
167 cells were used for phage amplification. Ninety-six randomly chosen clones among the

168 selected clones from round 3 were sequenced (Azenta, Cambridge, MA, USA).
169 Sequences were aligned, clustered and compared from one selection condition to the
170 others. Sequences common to at least 2 selection conditions were considered as non-
171 specific.

172 - *Cell culture and plasmid transfections*

173 HEK293A cells and HEK293/ΔGαs (22) were cultured in DMEM (Eurobio, Les Ulis,
174 France) supplemented with 10% (v/v) foetal bovine serum, 100 IU/mL penicillin, 0.1
175 mg/mL streptomycin (Eurobio, Les Ulis, France) and kept at 37°C in a humidified 5%
176 CO_2 incubator. Cells were transiently transfected in suspension using the Metafectene
177 Pro transfection reagent (Biontex Laboratories, München, Germany) following the
178 manufacturer's protocol. For interaction Bioluminescence resonance energy transfer
179 (BRET) experiments, cells were transiently co-transfected with plasmids encoding the
180 human FSHR-Rluc8 (0.1 µg plasmid DNA/cm^2) as BRET donor, and increasing
181 quantities of plasmids encoding the intra-VHH C-terminally fused to the Venus GFP-
182 derivative with a G4S linker as BRET acceptor (from 0 to 0.5 µg plasmid/cm^2). To have
183 an equivalent level of plasmid DNA transfected in all conditions, a pcDNA3.1 vector
184 encoding Venus alone was co-transfected. Further experiments are conducted with an
185 excess of VHH plasmid DNA in comparison to FSHR plasmid DNA transfected. For
186 Mini Gs protein recruitment BRET experiments, cells were transiently co-transfected
187 with plasmids encoding the human FSHR-Rluc8 (0.1 µg plasmid DNA/cm^2), the NES-
188 Venus-mGs (65 ng plasmid DNA/cm^2, kindly provided by Pr. Nevin A. Lambert,
189 Augusta University, Augusta, GA, USA) (23,24), and VHH-6xHis (0.2 µg plasmid
190 DNA/cm^2). For HTRF and flow cytometry experiments, 0.5 ng Flag-tagged human
191 FSHR (25) or 0.25 ng Flag-tagged human AVPR2 (26) plasmid DNA/cm^2 and 80 ng of
192 VHH-6xHis plasmid DNA/cm^2 were used for transfection. For the condition without
193 transfected VHH, an empty pcDNA3.1 plasmid was used. For confocal microscopy,
194 two quantities of intra-VHH-Venus were tested for transfection (0.3 or 0.45 µg plasmid
195 DNA/cm^2).

196 - *Cell imaging*

197 HEK293A cells were seeded on glass coverslips coated with Poly-L-Lysine (Sigma-
198 Aldrich, St. Louis, MO, USA) in 24-well plates. Cells were fixed in a solution of 4%
199 formaldehyde diluted in PBS for 10 min at room temperature, and washed six times in

200 PBS to remove formaldehyde. Hoechst stain was used to label cell nuclei (Sigma-
201 Aldrich, St. Louis, MO, USA). Following three PBS washes, coverslips were mounted
202 in Epredia™ Shandon™ Immu-Mount (Thermo Fisher Scientific, Waltham, MA, USA)
203 and left at room temperature overnight. Images were acquired on a ZEISS Axio
204 Observer Z1 using a 40X oil immersion objective and analysed with the ZEN software
205 (Zeiss, Oberkochen, Germany).

206 - *Flow Cytometry*

207 HEK293A cells transiently transfected with pcDNA3.1-VHH-6xHis plasmids were
208 detached following 1 hour-incubation in HBSS w/o Ca^{2+} (Eurobio, Les Ulis, France),
209 and re-suspended in working buffer (PBS w/o Ca^{2+} and Mg^{2+}, 0.5% BSA) 48 h after
210 transfection. Cells were then incubated with FcR Blocking Reagent human (1:20,
211 Miltenyi Biotech, Bergisch Gladbach, Germany) and LIVE/DEAD™ Fixable Violet Dead
212 Cell Stain (1:1000, Invitrogen, Waltham, MA, USA) for 10 min at 4°C. Cells were
213 washed twice in working buffer before permeabilization using BD Cytofix/Cytoperm™
214 Fixation/Permeabilization kit (BD Biosciences, Franklin Lakes, NJ, USA) following
215 manufacturer's protocol. APC-conjugated anti-6xHis antibody (His antibody APC,
216 1:1000, Miltenyi Biotech, Bergisch Gladbach, Germany) was added for 1 h at 4 °C.
217 Following two washes in perm/wash buffer, cells were resuspended in PBS for analysis
218 with the MACSQuant Analyzer 10 Flow cytometer (Miltenyi Biotech, Bergisch
219 Gladbach, Germany). Data were analyzed and plotted with the FlowJo software
220 (FlowJo, Ashland, OR, USA).

221 - *BRET assays*

222 Forty-eight hours after transfection, BRET measurements were performed upon
223 addition of 5 µM of coelenterazine H (Interchim, Montluçon, France) diluted in PBS for
224 non-stimulated conditions and upon addition of either 3.3 nM FSH or 100 nM AVP in
225 the presence of coelenterazine H for stimulated conditions to assay interaction.
226 Stimulation was performed upon addition of 33 nM FSH in the presence of
227 coelenterazine H for assaying Mini Gs protein recruitment. Signals were recorded for
228 20 min in a Mithras LB 943 plate reader (Berthold Technologies GmbH & Co., Wildbad,
229 Germany).

230 - *cAMP measurement by HTRF*

231 Forty-eight hours following transfection, cells were starved for 4 h in non-supplemented
232 DMEM. Cells were detached after a 1 hour-incubation in HBSS w/o Ca^{2+} at 37°C in a
233 humidified 5% CO_2 incubator. Cells were then dispatched in a 384 well-plate (Greiner
234 Bio-one, Courtaboeuf, France), stimulated for 15 min using either 2 µM forskolin (Fsk)
235 (MedChemExpress, South Brunswick, NJ, USA), 0.3 nM recombinant FSH (kindly
236 donated by Merck (Darmstadt, Germany), 0.25 nM arginine-vasopressin (AVP) (Tocris
237 Bioscience, Noyal Châtillon sur Seiche, France) or Isoproterenol hydrochloride (ISO)
238 (Sigma-Aldrich, St. Louis, MO, USA). Homogeneous time-resolved fluorescence
239 (HTRF) experiments were conducted using the cAMP Gs dynamic kit from Cisbio
240 (Waltham, Massachusetts, USA). After successive addition of the HTRF sensors, the
241 plate was incubated for 1 h at room temperature. Fluorescence measurement was then
242 performed with a TriStar² LB 942 Multimode Microplate Reader (Berthold Technologies
243 GmbH & Co., Wildbad, Germany).

244 - *Data analysis*

245 Data were representative of at least 4 independent experiments and were expressed
246 as mean values ± SEM. Data were analyzed and plotted using Graphpad Prism 9
247 (Graphpad Software Inc., San Diego, CA, USA). For interaction BRET, nonspecific
248 signal (when no VHH-Venus was expressed) was subtracted of the signal obtained
249 with T31 or iPRC1, and data were then normalized to T31 and fitted to a specific
250 binding curve with Hill slope (Graphpad Prism 9). For Mini Gs protein recruitment,
251 BRET data were expressed as a percentage of the maximal FSH-induced response in
252 the absence of VHH, and fitted to a one-phase association curve (Graphpad Prism 9).
253 For HTRF cAMP accumulation assay, data were normalized to forskolin-induced cAMP
254 accumulation and expressed as a percentage of ligand-induced response in the
255 absence of intra-VHH. Statistical significance was estimated by the Mann-Whitney test
256 to compare 2 different samples. Differences among means were considered significant
257 at $P < 0.05$. Image processing was performed with Fiji,(27).

258 - *In silico docking*

259 The model of the iPRC1 VHH was generated by homology modelling using SWISS-
260 MODEL (28–31). Docking of the iPRC1 CDR3 on the ICL3 of either inactive FSHR
261 (PDB: 812H) or activated FSH-FSHR-Gs complex (PDB: 812G) was performed using
262 the standard 'EASY' access settings on HADDOCK 2.4 (32,33). The generated

263 HADDOCK models were visualised, superimposed onto each other, and analysed
264 using the PyMOL Molecular Graphics System, Version 2.0 Schrödinger, LLC.

265 **Results**

266 ***Selection of the iPRC1 intra-VHH***

267 To select intra-VHH targeting the FSHR intra-cellular side, we performed phage display
268 on peptides corresponding to intracellular loops 1, 2 and 3 (ICL1, ICL2 and ICL3) of
269 the receptor (Figure 1). Following three rounds of selection, the common clones
270 identified in several conditions were considered as non-specific. Among the clones not
271 common to ICL1 and ICL2 selections, a VHH directed against the FSHR ICL3, iPRC1,
272 was selected through further analysis. An irrelevant intra-VHH T31, randomly picked
273 from a llama phage library and consistently observed as devoid of FSHR binding, has
274 been used as a negative control in all following experiments.

275 ***Expression of iPRC1 in mammalian cells***

276 In order to be functionally characterized, iPRC1 and T31 were transiently expressed in
277 HEK293A cells. We first assessed potential aggregation of the T31-Venus and iPRC1-
278 Venus intra-VHHs (Figure 2A). Using confocal microscopy, we detected no sign of
279 aggregation but rather homogeneous expression of both intra-VHHs, even with high
280 quantities of transfected plasmid DNA (450 ng of DNA per cm^2). Then the expression
281 level of the two intra-VHH C-terminally linked to a 6xHis-tag was assessed by flow
282 cytometry (Figure 2B), in all conditions of the following functional assays. Control and
283 iPRC1 intra-VHHs both exhibited comparable levels of expression.

284 ***iPRC1 binding to the FSHR***

285 Even though iPRC1 was selected on the FSHR ICL3, it was crucial to confirm its
286 binding to the full-length receptor in native conditions. Here, the interaction between
287 iPRC1 and the human FSHR was assayed by a BRET method using the VHH C-
288 terminally fused to the Venus BRET acceptor, and the FSHR or the arginine-
289 vasopressin 2 receptor (AVPR2) fused to the RLuc8 BRET donor. With increasing
290 amounts of transfected VHH-Venus plasmids (Figure 3A), a dose-dependent and
291 much higher binding of iPRC1 to FSHR than to AVPR2 was observed, even though a
292 weak binding signal was detected with AVPR2. There was no impact of the presence
293 of the ligand on iPRC1 binding, which indicates that iPRC1 has no preference for
294 inactive or ligand-induced active conformations of the FSHR. The maximum binding

295 estimated from fitting the data to specific binding curves with Hill slope showed a
296 statistically significant difference for FSHR, when compared to AVPR2 (Figure 3B).

297 ***Functional effect of iPRC1 on ligand-induced G protein-dependent signalling***

298 Knowing that ICL2 and ICL3 are important interfaces between Gα proteins and class
299 A GPCRs (6), we focused on G protein-dependent signalling. In order to predict
300 whether iPRC1 would interfere with the Gs protein/ FSHR interaction, we first
301 performed docking studies of a modelled iPRC1 CDR3 on the ICL3 of human FSHR
302 active or inactive structures. Docking of the iPRC1 CDR3 on the inactive FSHR led to
303 9 clusters, the best one consisting of 83 models, having HADDOCK score of -89.1 +/-
304 5.9 (Figure 4A). The HADDOCK score is the weighted sum of energies, with the most
305 negative values representing the most energetically favourable models. Although only
306 the CDR3 of iPRC1 was defined as the active residues in the interaction during the
307 docking process, the models generated also suggested the involvement of CDR1 and
308 CDR2. Visual inspection of models indicated several poses of iPRC1 with varying
309 vertical-horizontal orientations located on the external side of ICL3 (Figure 4A, left, for
310 a focused view, see Supplementary Figure 2). The superimposition of the best models
311 from the different clusters onto the FSH-FSHR-Gs complex indicated that the binding
312 of iPRC1 to ICL3 would cause steric clash with Gαs (Figure 4A, right, for a focused
313 view, see Supplementary Figure 2). The degree of steric clash with Gαs varied
314 according to the orientation of iPRC1, being minimized with the horizontal pose.
315 However, such horizontal poses could incur steric clashes with the cell membrane.
316 Steric hindrance between iPRC1 and Gs, and the cell membrane, was also confirmed
317 with the active FSH-FSHR-Gs complex, as the models generated did not provide good
318 HADDOCK scores: the best cluster consisted of only 17 models with HADDOCK score
319 of -1.6 +/- 25.1. Overall, it is clear from these models that iPRC1 was either targeting
320 intra-membrane portions of the FSHR or was in steric clash with the cell membrane.
321 Since these docking data suggest a competition between G proteins and iPRC1 upon
322 FSH binding, we next investigated whether iPRC1 would impact ligand-induced G
323 protein-dependant second messenger production. The outcome of iPRC1 or T31
324 intracellular expression was assayed on cAMP production that results from G protein
325 recruitment upon receptor activation, using HTRF (Figure 4). When compared to the
326 mock-transfected condition (no VHH transfected), iPRC1 induced a decrease of 33%
327 of cAMP accumulation in HEK293A cells transiently co-expressing the FSHR and the

328 intra-VHH, and stimulated for 15 min with 0.3 nM FSH. No effect of the T31 control
329 was observed in the same conditions (Figure 4B). The selectivity of iPRC1 was tested
330 on two other Gs-coupled class A GPCRs, structurally unrelated to the FSHR, the
331 AVPR2 and the beta 2 adrenergic receptor (ADRB2). The AVP-induced cAMP
332 production in HEK293A cells transiently expressing AVPR2, and stimulated for 15 min
333 with 0.25 nM AVP (Figure 4C), or the ISO-induced cAMP production in HEK293A cells
334 endogenously expressing ADRB2 (Figure 4D) were not altered by the co-expression
335 of T31 as expected, nor of iPRC1. These data show that iPRC1 negatively regulates
336 the FSH-induced Gs protein-dependent signalling, and this effect is specific of the anti-
337 FSHR intra-VHH selected in this study.

338 As suggested by the docking data, the reduced cAMP production in response to FSH
339 might be due to iPRC1 partially preventing Gs protein interaction with the receptor. To
340 verify this hypothesis, we assessed the recruitment of Mini Gs to the receptor in
341 absence or in presence of T31 or iPRC1 by BRET (Figure 4E). This experiment was
342 performed in HEK293/ΔGαs to avoid competition with the endogenous untagged Gs
343 proteins. The intracellular expression of iPRC1 slightly decreased Mini Gs/FSH-
344 activated FSHR BRET signal in comparison to T31 or mock conditions, but not
345 significantly, suggesting that iPRC1 does not compete with Gs for interaction with
346 FSHR.

347

348

349 **Discussion**

350 In this study, we have selected the first intra-VHH targeting a member of the
351 glycoprotein hormone receptor family, the FSHR, while only few VHHs targeting the
352 intracellular side of GPCRs have been functionally characterized to date. This intra-
353 VHH is directed against the FSHR ICL3 and impairs the cAMP production of the ligand-
354 bound receptor, despite the recruitment of Gαs. Thus, iPRC1 behaves as an allosteric
355 modulator of FSHR.

356 We first showed that iPRC1 was correctly expressed in mammalian cells and did not
357 aggregate, which makes it well suited for experiments in a cellular context. iPRC1
358 specifically recognized the FSHR, when compared to two other Gs-coupled GPCR,
359 AVPR2 and ADRB2. However, iPRC1 specificity towards the two other glycoprotein
360 hormone receptors, LHCGR and TSHR, which share high sequence similarity with the
361 FSHR, still remains to be assayed. Importantly, iPRC1 recognised the receptor
362 whether it is FSH-stimulated or not. Hence, iPRC1 is not specific of an inactive or an
363 FSH-activated conformation of the FSHR. G proteins are recruited to the FSHR notably
364 through the ERW motif present on ICL2, but also through a basic motif on ICL3 (21)
365 (Supplementary Figure 3). Therefore, iPRC1 might interfere with G protein interaction
366 with the FSHR through steric hindrance, a hypothesis supported by our docking results
367 that overall suggest direct steric clashes with Gαs. Consistently, iPRC1 specifically
368 reduced the FSH-induced cAMP production in HEK293 cells transiently expressing the
369 FSHR, but not the AVPR2 or the ADRB2 in the presence of their respective ligands.

370 From our results we anticipated a competition between iPRC1 and G proteins for
371 interaction with the receptor. Surprisingly, when the recruitment of mini Gs to the FSHR
372 was assayed in HEK293 cells depleted of Gαs protein, there was no significant impact
373 of the expression of iPRC1. The affinity of iPRC1 for the FSHR probably being weaker
374 than the affinity of G proteins for the receptor, the binding equilibrium might be in favour
375 of the G proteins. However, it does not explain the inhibitory effect of iPRC1 on cAMP
376 production. An alternative but not mutually exclusive hypothesis relies on the
377 observation that ICL3 is an allosteric site of major interest to modulate GPCR activity
378 and downstream signalling (34). This view probably applies to the FSHR since the
379 recently solved FSHR cryo-EM structure reveals a 14,9 Å movement of the N-term
380 portion of TM6 helix, suggesting the major importance of ICL3 in FSHR activation (16).

381 Therefore, by targeting ICL3, iPRC1 might affect FSHR helix conformational
382 transitions, hence activation. According to the docking studies, an interesting model for
383 the action of iPRC1 would be its binding to the external side of ICL3 in a horizontal
384 pose. Whilst steric clashes with Gαs is minimized, the presence of the iPRC1 however
385 limits the shift of the TM6 to allow for the full recruitment of Gαs since it would be
386 blocked by the cell membrane. This hypothesis is consistent with the binding data
387 suggesting that iPRC1 is able to interact with both active and inactive conformation of
388 FSHR. The Gs protein could also be recruited to the FSHR, but iPRC1 would imply a
389 reorientation that might not be optimal for its activation, thus explaining the reduction
390 of cAMP production.
391 The ICL3 length exhibits striking diversity among GPCRs, ranging from 10 to 240
392 amino-acids, and it has been recently proposed that this length might explain G protein
393 selectivity (34), the shorter the loop, the lower the selectivity. In this view, when bound
394 to the FSHR, whose ICL3 is only 23 amino acids long (against 47 and 55 amino acids
395 for AVPR2 and ADRB2 respectively), iPRC1 might promote coupling to other G
396 proteins (34).
397 ICL3 being also involved in the interaction of the receptor with β-arrestins, it would be
398 of major interest to study the impact of iPRC1 on β-arrestin-dependent signalling, for
399 example through direct β-arrestin recruitment.

400 Since it does not preferentially interact with an inactive or active conformation of the
401 FSHR, this intra-VHH is also a valuable tool to track FSHR trafficking in gonadal cells,
402 which has never been done before. In addition, an intra-VHH stabilizing a conformation
403 of specific interest could be used in reverse pharmacology. By stabilizing selective
404 conformations of a GPCR with an intra-VHH, it would be possible to screen and identify
405 extracellular binders that stabilize that same conformation and would be suited for
406 therapeutics purposes (35).

407 Ligand binding to its cognate GPCR results in a series of conformational changes that
408 propagate through the transmembrane domains, allowing the transmission of an
409 extracellular signal to the intracellular compartments of the cell. Although intra-VHH
410 have been instrumental to provide precious structural data on GPCRs, the extreme
411 complexity of GPCR signalling in correlation with conformational changes has not been
412 unravelled. Even though many published structures of GPCRs are available, they do
413 not provide a sufficient structural resolution of unstructured domains, such as the ICLs,

414 thus preventing any prediction of structure/ activity relationships. Therefore, intra-
415 VHHs that bind to ICLs and interfere with GPCR signalling pathways constitute
416 valuable tools to help complete structure/ activity studies performed so far.

Acknowledgements

The authors would like to acknowledge the Merck company for kindly providing purified recombinant human FSH, Pierre Martineau (Institut de Recherche en Cancérologie de Montpellier, France) for precious technical indications and for kindly providing the pCANTAB 6 phagemid vector and the KM13 helper phage.

Funding sources and disclosure of conflicts of interest

This work was funded with the support of Institut National de la Recherche Agronomique et de l'Environnement (INRAE), of the MAbImprove Labex (ANR-10-LABX-53) and of Région Centre Val de Loire ARD2020 Biomédicaments SELMAT grant and APR-IR INTACT grant.

PR was funded by a joint fellowship from Région Centre Val de Loire and INRAE PHASE Department. OV was funded by the APR-IR INTACT grant. AV, CaG and VJ was funded by the SELMAT grant of Région Centre Val de Loire ARD2020 Biomédicaments Program. CaG is co-funded by the INTACT grant from Région Centre Val de Loire. TB, ChG, GB and ER are funded by INRAE, FJ-A and PC are funded by the Centre National de la Recherche Scientifique (CNRS).

436 ## References

437 1. Latorraca NR, Venkatakrishnan AJ, Dror RO. GPCR Dynamics: Structures in Motion. Chem
438 Rev. 11 Jan 2017;117(1):139-55. doi:10.1021/acs.chemrev.6b00177

439 2. De Pascali F, Ayoub MA, Benevelli R, Sposini S, Lehoux J, Gallay N, et al. Pharmacological
440 Characterization of Low Molecular Weight Biased Agonists at the Follicle Stimulating
441 Hormone Receptor. Int J Mol Sci. 12 Sept 2021;22(18):9850. doi: 10.3390/ijms22189850

442 3. Stijlemans B, Conrath K, Cortez-Retamozo V, Van Xong H, Wyns L, Senter P, et al.
443 Efficient Targeting of Conserved Cryptic Epitopes of Infectious Agents by Single domain
444 Antibodies. J Biol Chem. Jan 2004;279(2):1256-61. doi:10.1074/jbc.M307341200

445 4. Liu H, Schittny V, Nash MA. Removal of a Conserved Disulfide Bond Does Not
446 Compromise Mechanical Stability of a VHH Antibody Complex. Nano Lett. 14 Aug
447 2019;19(8):5524-9. doi: 10.1021/acs.nanolett.9b02062

448 5. Manglik A, Kobilka B. The role of protein dynamics in GPCR function: insights from the
449 β2AR and rhodopsin. Curr Opin Cell Biol. Apr 2014;27:136-43. doi:
450 10.1016/j.ceb.2014.01.008.

451 6. Rasmussen SGF, Choi HJ, Fung JJ, Pardon E, Casarosa P, Chae PS, et al. Structure of a
452 nanobody-stabilized active state of the β2 adrenoceptor. Nature. Jan
453 2011;469(7329):175-80. doi:10.1038/nature09648

454 7. Kruse AC, Ring AM, Manglik A, Hu J, Hu K, Eitel K, et al. Activation and allosteric
455 modulation of a muscarinic acetylcholine receptor. Nature. 5 Dec 2013;504(7478):101-6.
456 doi: 10.1038/nature12735

457 8. Huang W, Manglik A, Venkatakrishnan AJ, Laeremans T, Feinberg EN, Sanborn AL, et al.
458 Structural insights into μ-opioid receptor activation. Nature. Aug
459 2015;524(7565):315-21. doi: 10.1038/nature14886

460 9. Masureel M, Zou Y, Picard LP, van der Westhuizen E, Mahoney JP, Rodrigues JPGLM, et
461 al. Structural insights into binding specificity, efficacy and bias of a β2AR partial agonist.
462 Nat Chem Biol. Nov 2018;14(11):1059-66. doi: 10.1038/s41589-018-0145-x

463 10. Staus DP, Strachan RT, Manglik A, Pani B, Kahsai AW, Kim TH, et al. Allosteric nanobodies
464 reveal the dynamic range and diverse mechanisms of G protein-coupled receptor
465 activation. Nature. July 2016;535(7612):448-52. doi: 10.1038/nature18636

466 11. Irannejad R, Tomshine JC, Tomshine JR, Chevalier M, Mahoney JP, Steyaert J, et al.
467 Conformational biosensors reveal GPCR signalling from endosomes. Nature. March
468 2013;495(7442):534-8. doi: 10.1038/nature12000

469 12. Raynaud P, Gauthier C, Jugnarain V, Jean-Alphonse F, Reiter E, Bruneau G, et al.
470 Intracellular VHHs to monitor and modulate GPCR signaling. Front Endocrinol. 16 Nov
471 2022;13:1048601. doi: 10.3389/fendo.2022.1048601

472 13. Staus DP, Wingler LM, Strachan RT, Rasmussen SGF, Pardon E, Ahn S, et al. Regulation of
473 β_2-Adrenergic Receptor Function by Conformationally Selective Single-domain
474 Intrabodies. Mol Pharmacol. March 2014;85(3):472-81. doi: 10.1124/mol.113.089516

475 14. McMahon C, Baier AS, Pascolutti R, Wegrecki M, Zheng S, Ong JX, et al. Yeast surface
476 display platform for rapid discovery of conformationally selective nanobodies. Nat Struct
477 Mol Biol. March 2018;25(3):289-96. doi: 10.1038/s41594-018-0028-6

478 15. Gromoll J, Simoni M, Nordhoff V, Behre HM, De Geyter C, Nieschlag E. Functional and
479 clinical consequences of mutations in the FSH receptor. Mol Cell Endocrinol. Dec
480 1996;125(1-2):177-82. doi: 10.1016/s0303-7207(96)03949-4

481 16. Duan J, Xu P, Zhang H, Luan X, Yang J, He X, et al. Mechanism of hormone and allosteric
482 agonist mediated activation of follicle stimulating hormone receptor. Nat Commun. 31
483 Jan 2023;14(1):519. doi: 10.1038/s41467-023-36170-3

484 17. Marion S, Robert F, Crepieux P, Martinat N, Troispoux C, Guillou F, et al. G Protein-
485 Coupled Receptor Kinases and Beta Arrestins Are Relocalized and Attenuate Cyclic 3′,5′-
486 Adenosine Monophosphate Response to Follicle-Stimulating Hormone in Rat Primary
487 Sertoli Cells. Biol Reprod. 1 Jan 2002;66(1):70-6. doi: 10.1095/biolreprod66.1.70

488 18. Marion S, Kara E, Crepieux P, Piketty V, Martinat N, Guillou F, et al. G protein-coupled
489 receptor kinase 2 and β-arrestins are recruited to FSH receptor in stimulated rat primary
490 Sertoli cells. J Endocrinol. Aug 2006;190(2):341-50. doi: 10.1677/joe.1.06857

491 19. Reiter E, Lefkowitz RJ. GRKs and beta-arrestins: roles in receptor silencing, trafficking and
492 signaling. Trends Endocrinol Metab. June 2006;17(4):159-65. doi:
493 10.1016/j.tem.2006.03.008

494 20. Sposini S, Jean-Alphonse FG, Ayoub MA, Oqua A, West C, Lavery S, et al. Integration of
495 GPCR Signaling and Sorting from Very Early Endosomes via Opposing APPL1 Mechanisms.
496 Cell Rep. Dec 2017;21(10):2855-67. doi: 10.1016/j.celrep.2017.11.023

497 21. Ulloa-Aguirre A, Zariñán T, Jardón-Valadez E, Gutiérrez-Sagal R, Dias JA. Structure-
498 Function Relationships of the Follicle-Stimulating Hormone Receptor. Front Endocrinol
499 29 Nov 2018. doi: 10.3389/fendo.2018.00707

500 22. Stallaert W, Van Der Westhuizen ET, Schönegge AM, Plouffe B, Hogue M, Lukashova V, et
501 al. Purinergic Receptor Transactivation by the β_2-Adrenergic Receptor Increases
502 Intracellular Ca^{2+} in Nonexcitable Cells. Mol Pharmacol. May 2017;91(5):533-44. doi:
503 10.1124/mol.116.106419

504 23. Ayoub MA, Landomiel F, Gallay N, Jégot G, Poupon A, Crépieux P, et al. Assessing
505 Gonadotropin Receptor Function by Resonance Energy Transfer-Based Assays. Front
506 Endocrinol. 27 Aug 2015;6. doi: 10.3389/fendo.2015.00130

507 24. Wan Q, Okashah N, Inoue A, Nehmé R, Carpenter B, Tate CG, et al. Mini G protein probes
508 for active G protein–coupled receptors (GPCRs) in live cells. J Biol Chem. May
509 2018;293(19):7466-73. doi: 10.1074/jbc.RA118.001975

510 25. Tranchant T, Durand G, Gauthier C, Crépieux P, Ulloa-Aguirre A, Royère D, et al.
511 Preferential β-arrestin signalling at low receptor density revealed by functional
512 characterization of the human FSH receptor A189 V mutation. Mol Cell Endocrinol. 1 Jan
513 2011;331(1):109-18. doi: 10.1016/j.mce.2010.08.016

514 26. Heitzler D, Durand G, Gallay N, Rizk A, Ahn S, Kim J, et al. Competing G protein-coupled
515 receptor kinases balance G protein and β-arrestin signaling. Mol Syst Biol. Jan
516 2012;8(1):590. doi: 10.1038/msb.2012.22

517 27. Schindelin J, Arganda-Carreras I, Frise E, Kaynig V, Longair M, Pietzsch T, et al. Fiji: an
518 open-source platform for biological-image analysis. Nat Methods. July 2012;9(7):676-82.
519 doi: 10.1038/nmeth.2019

520 28. Bertoni M, Kiefer F, Biasini M, Bordoli L, Schwede T. Modeling protein quaternary
521 structure of homo- and hetero-oligomers beyond binary interactions by homology. Sci
522 Rep. 5 Sept 2017;7(1):10480. doi: 10.1038/s41598-017-09654-8

523 29. Bienert S, Waterhouse A, de Beer TAP, Tauriello G, Studer G, Bordoli L, et al. The SWISS-
524 MODEL Repository—new features and functionality. Nucleic Acids Res. 4 Jan
525 2017;45(D1):D313-9. doi: 10.1093/nar/gkw1132

526 30. Waterhouse A, Bertoni M, Bienert S, Studer G, Tauriello G, Gumienny R, et al. SWISS-
527 MODEL: homology modelling of protein structures and complexes. Nucleic Acids Res. 2
528 July 2018;46(W1):W296-303. doi: 10.1093/nar/gky427

529 31. Studer G, Rempfer C, Waterhouse AM, Gumienny R, Haas J, Schwede T. QMEANDisCo—
530 distance constraints applied on model quality estimation. Bioinformatics. 1 March
531 2020;36(6):1765-71. doi: 10.1093/bioinformatics/btaa058

532 32. Van Zundert GCP, Rodrigues JPGLM, Trellet M, Schmitz C, Kastritis PL, Karaca E, et al. The
533 HADDOCK2.2 Web Server: User-Friendly Integrative Modeling of Biomolecular
534 Complexes. J Mol Biol. Feb 2016;428(4):720-5. doi: 10.1016/j.jmb.2015.09.014

535 33. Honorato RV, Koukos PI, Jiménez-García B, Tsaregorodtsev A, Verlato M, Giachetti A, et
536 al. Structural Biology in the Clouds: The WeNMR-EOSC Ecosystem. Front Mol Biosci. 28
537 July 2021;8:729513. doi: 10.3389/fmolb.2021.729513

538 34. Sadler F, Ma N, Ritt M, Sharma Y, Vaidehi N, Sivaramakrishnan S. Autoregulation of GPCR
539 signalling through the third intracellular loop. Nature. 23 March 2023;615(7953):734-41.
540 doi: 10.1038/s41586-023-05789-z

541 35. Pardon E, Betti C, Laeremans T, Chevillard F, Guillemyn K, Kolb P, et al. Nanobody-
542 Enabled Reverse Pharmacology on G-Protein-Coupled Receptors. Angew Chem Int Ed. 4
543 May 2018;57(19):5292-5. doi: 10.1002/anie.201712581

544

545

546

547 **Figure legends**

548 **Figure 1**: ***iPRC1 selection workflow.*** A phage library was constructed following llama
549 immunization by injection of a cDNA encoding the hFSHR. Selection was done by
550 phage display on the peptides corresponding to the FSHR intracellular loops, ICL1,
551 ICL2 and ICL3. Ninety-six randomly selected clones were sequenced for each
552 condition, and after sequence comparison of the selected clones in each conditions,
553 VHHs were selected.

554 **Figure 2*: iPRC1 and irrelevant T31 intra-VHH expression in HEK293A cells*. (A)**
555 Confocal microscopy representative images of T31-Venus (a and b) and iPRC1-Venus
556 (c and d) transiently expressed in HEK293A cells, using two quantities of plasmid DNA
557 (b and d). The intra-VHH-Venus is shown in green and the DAPI-stained nuclei**(B)** Flow
558 cytometry histograms showing the population of cells expressing either the irrelevant
559 intra-VHH T31-6xHis or iPRC1-6xHis (in red) in comparison to "mock"-cells transfected
560 with empty pcDNA3.1 vector (in blue).

561 **Figure 3**: ***iPRC1 associates to the FSHR, whether FSH is present or not.* (A)**
562 Bioluminescence resonance energy transfer (BRET) binding assay between FSHR-
563 RLuc8 and increasing amounts of transfected iPRC1-Venus plasmid. Experiments
564 were done in the absence of ligand or in the presence of 3.3 nM FSH or 100 nM AVP,
565 as indicated. BRET ratios (at 2 min following FSH addition) were normalized to the
566 BRET ratios obtained in the presence of the irrelevant T31-Venus intra-VHH. Data are
567 represented as mean ± SEM, and the curves correspond to fitted data to specific
568 binding curves with Hill slope, N=4. **(B)** Comparison of the estimated maximum binding
569 obtained for iPRC1 to the FSHR to the estimated maximum binding value obtained for
570 iPRC1 association to AVPR2. Data are represented as mean ± SEM. Statistical
571 significance was assessed by unpaired Mann-Whitney test, N = 4, * $p < 0.05$.

572 **Figure 4**: ***iPRC1 expression affects G protein signalling pathway.* (A)** iPRC1 CDR3
573 molecular docking to hFSHR ICL3. *Left:* Models of inactive FSHR (PDB: 8I2H) with 2
574 examples of iPRC1 poses. *Right*: Models of inactive FSHR (PDB: 8I2H)-iPRC1
575 superimposed onto FSHR-FSH-Gαs (PDB: 8I2G) (for simplicity, FSH, Gβ, Gγ and
576 Nb35 are not shown). Homogeneous time-resolved fluorescence (HTRF) cAMP
577 accumulation assay in HEK293A cells transiently expressing the FSHR **(B)** or AVPR2
578 **(C),** or endogenously expressing ADRB2 **(D)**, and transiently expressing either T31 or

579 iPRC1, stimulated with 0.25 nM AVP (N=4), 0.3 nM FSH (N=6) or 0.2 μM ISO (N=4)
580 for 15 min. For each receptor, data were normalized to the cAMP response to Fsk and
581 represented as the percentage of the cAMP response to FSH in the absence of
582 transfected VHH. Statistical significance between the mean ± SEM was assessed by
583 unpaired Mann-Whitney test, N = 6, ** $p < 0.01$. **(E)** Bioluminescence resonance
584 energy transfer (BRET) assay measuring the recruitment of NES-Venus-mGs to
585 FSHR-RLuc8, in presence of either T31 or iPRC1, in response to cells stimulation with
586 33 nM FSH. BRET ratios were expressed as percentage of the maximal FSH-response
587 in the absence of VHH. Data are represented as mean ± SEM, and curves correspond
588 to fitted data to one-phase association curves, N = 4.

589

590

Figure 1

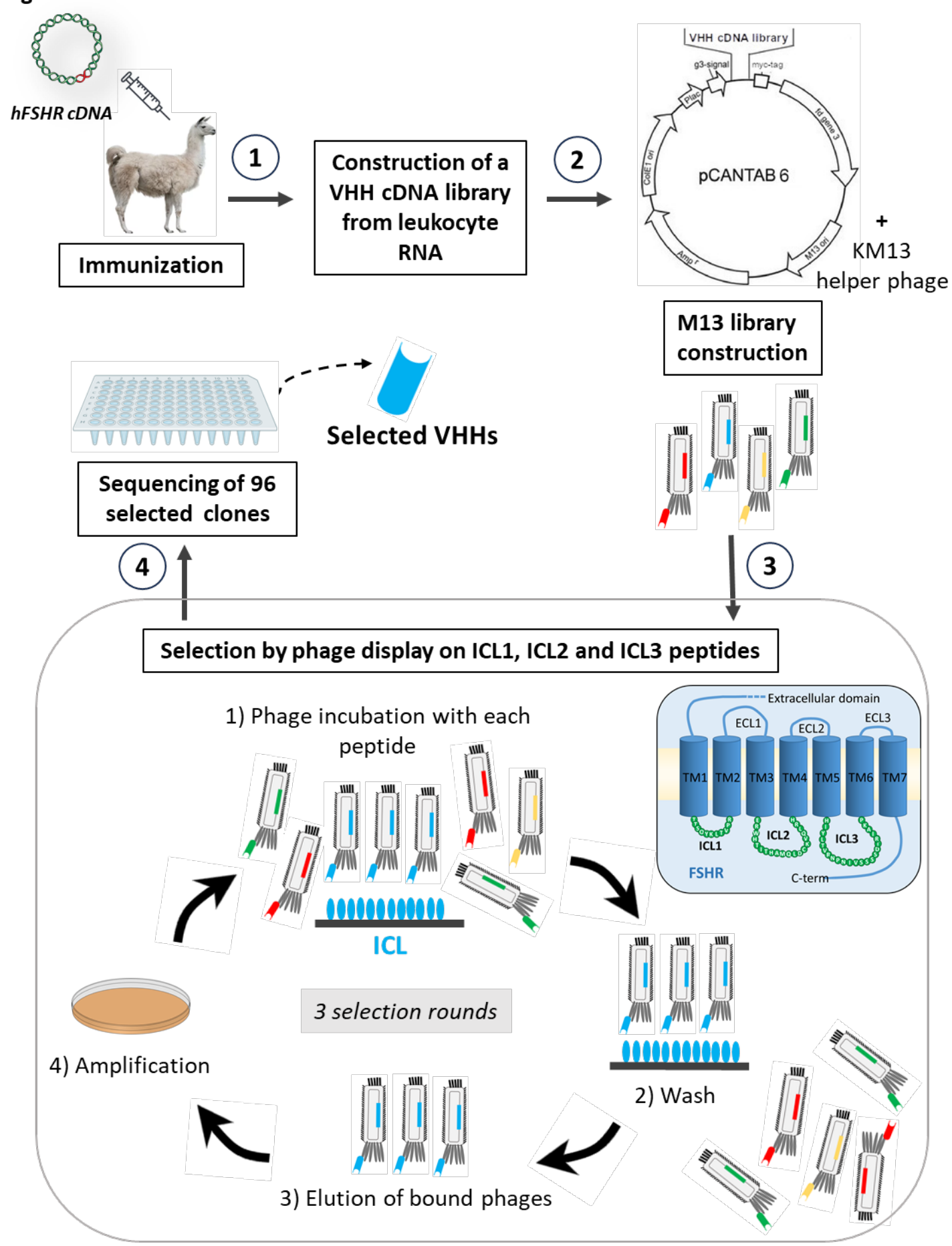
hFSHR cDNA
Immunization
1
Construction of a VHH cDNA library from leukocyte RNA
2
VHH cDNA library
g3-signal
myc-tag
Plac
pCANTAB 6
+
KM13 helper phage
M13 library construction
Selected VHHs
Sequencing of 96 selected clones
4
3
Selection by phage display on ICL1, ICL2 and ICL3 peptides
1) Phage incubation with each peptide
Extracellular domain
ECL1
ECL2
ECL3
TM1
TM2
TM3
TM4
TM5
TM6
TM7
ICL1
ICL2
ICL3
FSHR
C-term
ICL
3 selection rounds
2) Wash
3) Elution of bound phages
4) Amplification

Figure 2

A

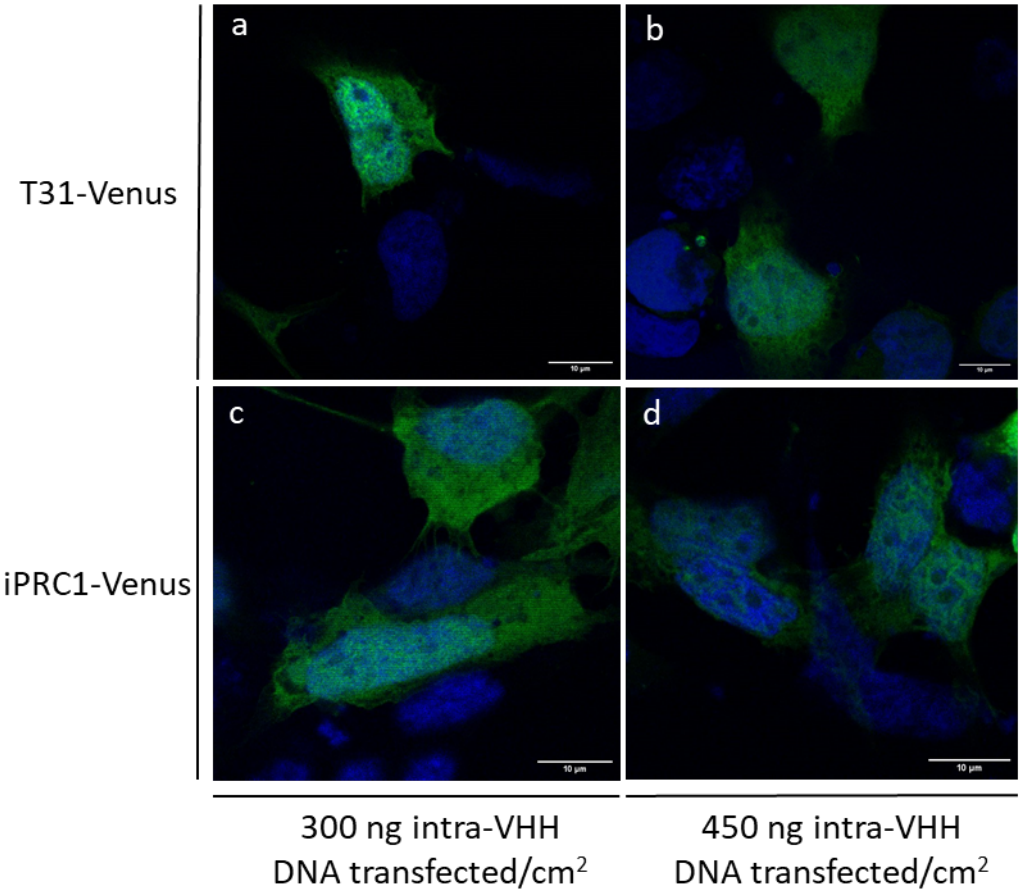

B

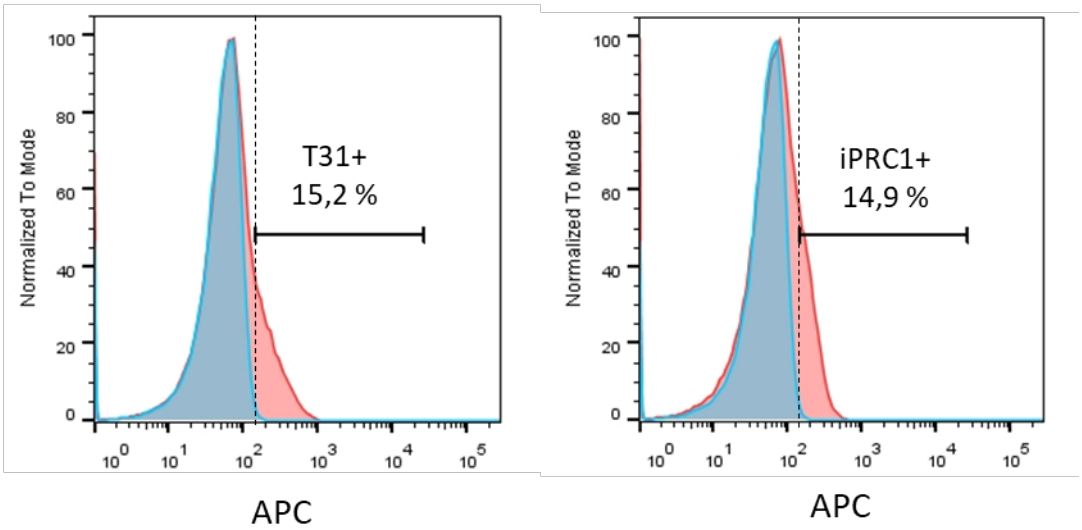

591

Figure 3

592

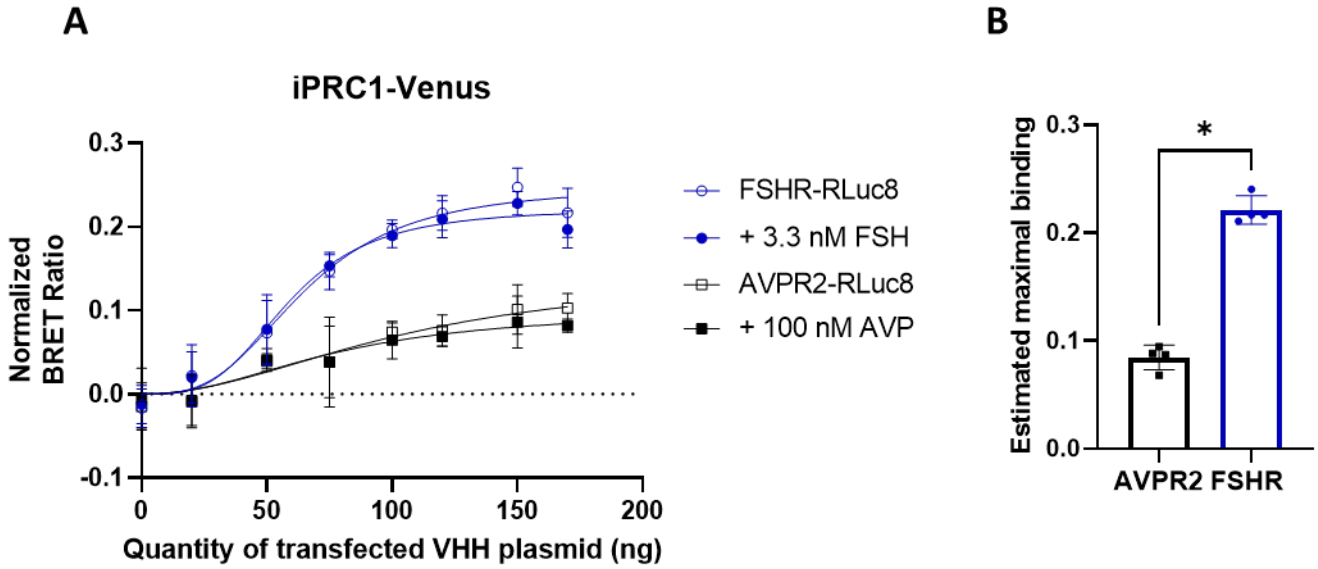
A
iPRC1-Venus
Normalized BRET Ratio
0.3
0.2
0.1
0.0
-0.1
0
50
100
150
200
Quantity of transfected VHH plasmid (ng)
FSHR-RLuc8
+ 3.3 nM FSH
AVPR2-RLuc8
+ 100 nM AVP
B
Estimated maximal binding
0.3
0.2
0.1
0.0
*
AVPR2
FSHR

593

Figure 4

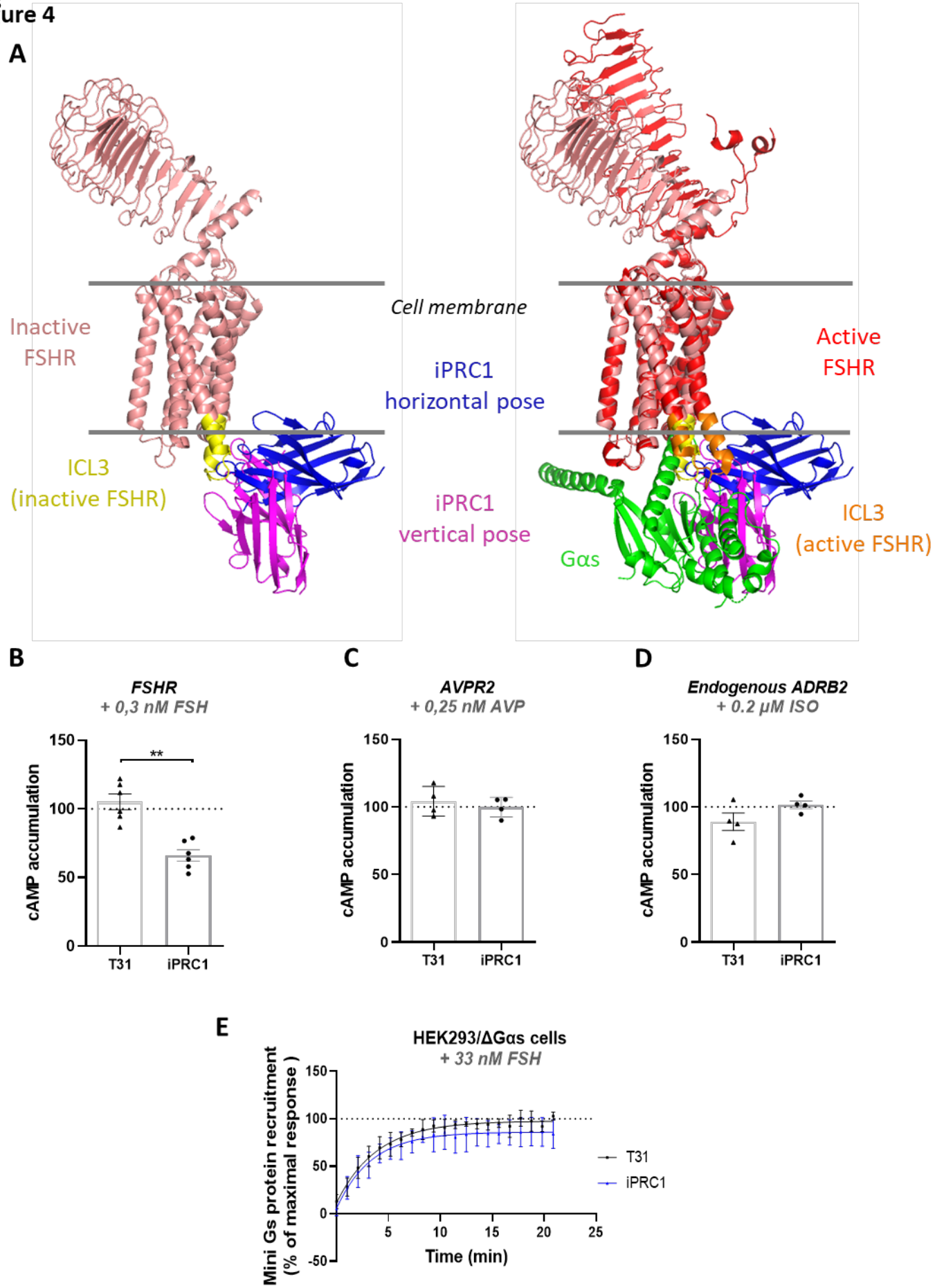
A
Inactive FSHR
ICL3 (inactive FSHR)
Cell membrane
iPRC1 horizontal pose
iPRC1 vertical pose
Active FSHR
ICL3 (active FSHR)
Gαs
B
FSHR
+ 0,3 nM FSH
cAMP accumulation
150
100
50
0
**
T31
iPRC1
C
AVPR2
+ 0,25 nM AVP
cAMP accumulation
150
100
50
0
T31
iPRC1
D
Endogenous ADRB2
+ 0.2 µM ISO
cAMP accumulation
150
100
50
0
T31
iPRC1
E
HEK293/ΔGαs cells
+ 33 nM FSH
Mini Gs protein recruitment (% of maximal response)
150
100
50
0
-50
5
10
15
20
25
Time (min)
T31
iPRC1